Proceedings of the International Conference of Control, Dynamic Systems, and Robotics
Ottawa, Ontario, Canada, May 15-16 2014
Paper No. 94

Coordination Control with Collision Avoidance for Multiagent Systems with Underactuated Agent Dynamics

Masood Ghasemi, Sergey G. Nersesov, Garrett Clayton, and Hashem Ashrafiuon
Department of Mechanical Engineering
Center for Nonlinear Dynamics and Control (CENDAC)
Villanova University
800 Lancaster Avenue, Villanova, PA 19085, USA
mghase01@villanova.edu; sergey.nersesov@villanova.edu; garrett.clayton@villanova.edu;
hashem.ashrafiuon@villanova.edu

Abstract - A coordinated control framework for multiagent systems using sliding mode control approach was developed in (Ghasemi and Nersesov, 2013). The framework addresses a general class of underactuated agents and presents a specialization to the agents represented by wheeled mobile robots. In this paper, we extend the results of (Ghasemi and Nersesov, 2013) to incorporate the obstacle/collision avoidance algorithm into the overall coordination control routine. Obstacle avoidance is achieved by surrounding the stationary as well as moving obstacles by elliptical or other convex shapes that serve as stable periodic solutions to planar systems of ordinary differential equations and using transient trajectories of those systems to navigate the agents around the obstacles. We experimentally validate the efficacy of our theoretical approach using two wheeled mobile robots that reach and maintain a desired formation in the presence of the obstacles while avoiding collisions.

Keywords: multiagent systems, underactuated systems, sliding mode control, collision avoidance.

1. Introduction

Research on analysis and control design for networks of mobile agents has grown overwhelmingly over the past few decades. Some of the most relevant references to the results presented in this paper include (Porfiri et al., 2007; Ren and Beard, 2008; Bullo et al., 2009) where the authors develop a variety of control algorithms for network consensus. The most common manoeuvres that a group of mobile agents may perform are flocking, cyclic pursuit , (virtual) leader following, and rendezvous. However, many of the existing results use single- or double-integrator agent models to validate the developed approaches without taking into account complex internal dynamics of individual agents including various kinematic constraints such as, for example, non-holonomic constraints for wheeled mobile robots or second-order non-holonomic constraints for surface vessels.

In (Ghasemi and Nersesov, 2013), we consider coordinated motion of an ensemble of agents characterized by general underactuated nonlinear dynamics and develop cooperative control algorithm using sliding mode control approach. We use graph theoretic notions to characterize the formation and in the directed graph we identify a spanning tree (Bullo et al., 2009) to characterize the minimum set of communication links among the agents required to ensure a weakly connected directed graph. Decentralized controllers for individual agents are based on the sliding mode control technique (Utkin, 1977) and use only local information from the agent itself and a neighboring agent from the spanning tree that communicates its state

information directly to this agent.

In this paper, we extend the results of (Ghasemi and Nersesov, 2013) to incorporate an obstacle avoidance technique that is based on encircling the obstacles by elliptical shapes which serve as stable limit cycles of planar systems of ordinary differential equations (Soltan et al., 2011). We identify a safety zone around an obstacle that is of similar elliptical shape which encloses the limit cycle such that when an agent enters this zone, the individual control strategy for this agent switches to the transient control strategy that drives this agent towards the limit cycle. Due to uniqueness of solutions to the systems of ordinary differential equations, the agent position never crosses into the limit cycle thus guaranteeing safe bypassing of an obstacle. Once the obstacle is cleared, the individual control strategy switches back to the cooperative control strategy aimed at maintaining the desired formation for the multiagent system. The developed framework also addresses moving obstacles including agents themselves which ensures collision avoidance. We validate our results experimentally using two wheeled mobile robots performing a coordinated motion.

2. Mathematical Preliminaries

In this section, we present some basic definitions from the graph theory. A *directed graph* or *digraph* G of order n is a pair $(\mathscr{V},\mathscr{E})$, where $\mathscr{V}$ (*vertex set*) is a set of n elements called *vertices* (or *nodes*) and $\mathscr{E}$ (*edge set*) is a set of ordered pairs of vertices called edges. For $u,v \in \mathscr{V}(G)$, the ordered pair $(u,v) \in \mathscr{E}(G)$ denotes an edge from u to v. We assume that $u \neq v$ for any $(u,v) \in \mathscr{E}(G)$, that is, the graph has no self-loops. If $(u,v) \in \mathscr{E}(G)$ implies $(v,u) \in \mathscr{E}(G)$ for any $(u,v) \in \mathscr{E}(G)$, then the graph is called *undirected graph* or simply *graph*.

A *path* on graph G of length m from $u_0 \in \mathscr{V}(G)$ to $u_m \in \mathscr{V}(G)$ is an ordered set of distinct vertices $\{u_0,\ldots,u_m\}$ such that any pair of consecutive vertices $(u_{i-1},u_i) \in \mathscr{E}(G)$ for all $i = 1,\ldots,m$. A *directed path* on a digraph G of length m from $u_0 \in \mathscr{V}(G)$ to $u_m \in \mathscr{V}(G)$ is an ordered set of distinct vertices $\{u_0,\ldots,u_m\}$ such that any directed pair of consecutive vertices $(u_{i-1},u_i) \in \mathscr{E}(G)$ for all $i = 1,\ldots,m$. A graph G is *connected* if there exists a path between any two of its vertices. A digraph G is *strongly connected* if there exists a directed path between any two of its vertices. Also, a digraph G is *weakly connected* if it is not strongly connected and its associated undirected graph obtained by removing directions on edges is connected.

A *directed tree* is a weakly connected digraph containing one source such that the in-degree of its other vertices is one. A *directed spanning tree* or simply a *spanning tree* of a digraph is a spanning subgraph that is a directed tree (Bullo et al., 2009).

3. Obstacle and Collision Avoidance

A general coordinated control framework for multiagent systems using sliding mode control approach was developed in (Ghasemi and Nersesov, 2013). The framework addresses a general class of underactuated systems whose individual dynamics are given by

$$\dot{x}_{1i}(t) = f_{1i}(t,x_i(t)), \quad x_{1i}(0) = x_{1i0}, \quad i = 1,\ldots,p, \quad t \geq 0, \tag{1}$$

$$\dot{x}_{2i}(t) = f_{2i}(t,x_i(t)) + B_{2i}(t,x_i(t))u(t) + g_i(t,x_i(t)), \quad x_{2i}(0) = x_{2i0}, \tag{2}$$

where $x_{1i} \in \mathbb{R}^{n-m}$, $x_{2i} \in \mathbb{R}^m$, $x_i \triangleq [x_{1i}^{\mathrm{T}},x_{2i}^{\mathrm{T}}]^{\mathrm{T}} \in \mathbb{R}^n$ are the state variables of the ith agent, $u_i(t) \in \mathbb{R}^m$, $t \geq 0$, is the control input for the ith agent, $f_{1i}(t,x_i) \in \mathbb{R}^{n-m}$ and $f_{2i}(t,x_i) \in \mathbb{R}^m$ represent the internal dynamics of the ith agent, $B_{2i}(t,x_i) \in \mathbb{R}^{m\times m}$ is invertible, and $g_i(t,x_i) \in \mathbb{R}^m$ represents the vector of bounded uncertainties and disturbances affecting the dynamics of the ith agent.

In this paper, we extend the results of (Ghasemi and Nersesov, 2013) to address obstacle and collision avoidance in the context of coordinated motion and specialize these results to the multiagent systems composed of wheeled mobile robots whose individual dynamics are given in (Ghasemi and Nersesov, 2013). In

particular, we develop an obstacle avoidance algorithm using the idea presented in (Soltan et al., 2011). In this approach, every obstacle, including moving obstacles, is enclosed by an ellipsoid which also serves as a stable limit cycle for a planar system of ordinary differential equations. The idea is as follows, when an agent appears in a close vicinity of an obstacle, the decentralized cooperative control algorithm developed in (Ghasemi and Nersesov, 2013) switches to the obstacle avoidance algorithm driving the agent towards the periodic orbit enclosing the obstacle. Eventually, as soon as the obstacle is cleared, the agent switches back to the coordination algorithm leading the agent to its desired path. We assume that the agents are initially outside the periodic orbits enclosing all obstacles such that our algorithm ensures obstacle avoidance for all times. Note that each agent can be considered as an obstacle for other agents, therefore our obstacle avoidance algorithm also ensures collision avoidance.

To elucidate our obstacle avoidance algorithm, consider an individual agent i whose dynamics are given by (1), (2) and define the error states with respect to the jth obstacle as

$$\tilde{z}_{ij}(t) \triangleq x_{1i}(t)-\tilde{x}_j(t), \quad j\in\mathscr{O}, \quad t\geq 0, \tag{3}$$

where $\tilde{z}_{ij}\in\mathbb{R}^{n-m}$, $\tilde{x}_j\in\mathbb{R}^{n-m}$ is the center position of the jth obstacle, and $\mathscr{O}$ is a set containing all obstacles in the workspace. Accordingly, the error dynamics of the ith agent is given by

$$\dot{\tilde{z}}_{ij}(t) = f_{1i}(t,\tilde{z}_{ij},x_{2i},\tilde{x}_j(t))-\dot{\tilde{x}}_j(t), \quad \tilde{z}_i(0)=\tilde{z}_{i0}, \quad j\in\mathscr{O} \quad t\geq 0, \tag{4}$$

$$\dot{x}_{2i}(t) = f_{2i}(t,\tilde{z}_{ij},x_{2i},\tilde{x}_j(t))+B_{2i}(t,\tilde{z}_{ij},x_{2i},\tilde{x}_j(t))u_i(t)+g_i(t,\tilde{z}_{ij},x_{2i},\tilde{x}_j(t)), \quad x_{2i}(0)=x_{2i0}. \tag{5}$$

Next, we present a general structure for the sliding surface and the corresponding sliding mode control such that the closed-loop dynamics restricted to the sliding surface exhibit periodic behavior. Consider a vector function $\sigma_{ij}:\overline{\mathbb{R}}_+\times\mathbb{R}^{(n-m)}\times\mathbb{R}^m\times\mathbb{R}^{n-m}\to\mathbb{R}^m$ given by

$$\begin{aligned}\sigma_{ij}(t,\tilde{z}_{ij},x_{2i},\tilde{x}_j(t)) \triangleq\ & S_{1ij}(t,\tilde{z}_{ij})x_{2i}(t)-S_{2ij}(t,\tilde{z}_{ij})\dot{\tilde{x}}_j(t)+\tilde{\sigma}_{ij}(t,\tilde{z}_{ij}),\\ & (t,\tilde{z}_{ij},x_{2i},\tilde{x}_j(t))\in\overline{\mathbb{R}}_+\times\mathbb{R}^{(n-m)}\times\mathbb{R}^m\times\mathbb{R}^{n-m},\end{aligned} \tag{6}$$

where $S_{1ij}:\overline{\mathbb{R}}_+\times\mathbb{R}^{(n-m)}\to\mathbb{R}^{m\times m}$ is invertible, $S_{2ij}:\overline{\mathbb{R}}_+\times\mathbb{R}^{(n-m)}\to\mathbb{R}^{m\times(n-m)}$, $\tilde{\sigma}_{ij}:\overline{\mathbb{R}}_+\times\mathbb{R}^{(n-m)}\to\mathbb{R}^m$. We define the ith sliding surface as the null space of $\sigma_{ij}(\cdot,\cdot,\cdot,\cdot)$, that is,

$$\mathscr{S}_i\triangleq\{(t,\tilde{z}_{ij},x_{2i},\tilde{x}_j(t))\in\overline{\mathbb{R}}_+\times\mathbb{R}^{(n-m)}\times\mathbb{R}^m\times\mathbb{R}^{n-m}:\ \sigma_{ij}(t,z_i,x_{2i},x_{2j})=0\}. \tag{7}$$

The sliding mode control law u_i is calculated by setting $\dot{\sigma}_i(t,\tilde{z}_{ij},x_{2i},\tilde{x}_j(t))=0,\ j\in\mathscr{O}$, for the nominal system and adding a signum function to ensure finite-time convergence to the sliding surface. Specifically, using (4), (5) and (6), we set

$$\begin{aligned}u_i(t) = & -B_{2i}^{-1}(t,\tilde{z}_{ij})S_{1ij}^{-1}(t,\tilde{z}_{ij})[S_{1ij}(t,\tilde{z}_{ij})f_{2i}(t,\tilde{z}_{ij},x_{2i},\tilde{x}_j(t))+\dot{S}_{1ij}(t,\tilde{z}_{ij})x_{2i}(t)\\ & -\dot{S}_{2ij}(t,\tilde{z}_{ij})\dot{\tilde{x}}_j(t)-S_{2ij}(t,\tilde{z}_{ij})\ddot{\tilde{x}}_j(t)+\dot{\tilde{\sigma}}_{ij}(t,\tilde{z}_{ij})+\tilde{K}_{ij}\,\mathrm{sign}(\sigma_{ij}(t,\tilde{z}_{ij},x_{2i},\tilde{x}_j(t)))],\end{aligned} \tag{8}$$

where

$$\mathrm{sign}(\sigma_{ij}(t,\tilde{z}_{ij},x_{2i},\tilde{x}_j(t))) \triangleq \begin{bmatrix}\mathrm{sign}(\sigma_{ij1}(t,\tilde{z}_{ij},x_{2i},\tilde{x}_j(t)))\\ \vdots\\ \mathrm{sign}(\sigma_{ijm}(t,\tilde{z}_{ij},x_{2i},\tilde{x}_j(t)))\end{bmatrix}^{\mathrm{T}}, \tag{9}$$

$\sigma_{ijk}(\cdot,\cdot,\cdot,\cdot)$, $k=1,\ldots,m$, is the kth component of $\sigma_{ij}(\cdot,\cdot,\cdot,\cdot)$, and $\tilde{K}_{ij}\triangleq\mathrm{diag}\,[\tilde{k}_{ij1},\ldots,\tilde{k}_{ijm}]$,

$$\tilde{k}_{ijk}=\tilde{\lambda}_{ijk}+\sup_{(t,\tilde{z}_{ij},x_{2i},\tilde{x}_j(t))\in\overline{\mathbb{R}}_+\times\mathbb{R}^{n-m}\times\mathbb{R}^m\times\mathbb{R}^{n-m}}\|g_i(t,\tilde{z}_{ij},x_{2i},\tilde{x}_j(t))\|_\infty, \tag{10}$$

with $\tilde{\lambda}_{ijk} > 0$, $i = 1,\ldots,p$, $j \in \mathscr{O}$, $k = 1,\ldots,m$.

Next, we show that with the feedback control law (8), the trajectories of the closed-loop system (4), (5) converge to the sliding surface (7) in finite time. To see this, consider a Lyapunov function candidate given by

$$V_i(\sigma_{ij}(t,\tilde{z}_{ij},x_{2i},\tilde{x}_j(t))) \;=\; \sigma_{ij}^{\mathrm{T}}(t,\tilde{z}_{ij},x_{2i},\tilde{x}_j(t))\sigma_{ij}(t,\tilde{z}_{ij},x_{2i},\tilde{x}_j(t)), \quad \sigma_{ij}(t,\tilde{z}_{ij},x_{2i},\tilde{x}_j(t)) \in \mathbb{R}^m. \quad (11)$$

Note that $V_i(\sigma(t,\tilde{z}_{ij},x_{2i},\tilde{x}_j(t))) = 0$, $(t,\tilde{z}_{ij},x_{2i},\tilde{x}_j(t)) \in \mathscr{S}_i$, and $V_i(\sigma(t,\tilde{z}_{ij},x_{2i},\tilde{x}_j(t))) > 0$, $(t,\tilde{z}_{ij},x_{2i},\tilde{x}_j(t)) \notin \mathscr{S}_i$. Furthermore, it can be shown that the Lyapunov derivative along the trajectories of the closed-loop system satisfies

$$\dot{V}_i(\sigma(t,\tilde{z}_{ij},x_{2i},\tilde{x}_j(t))) \;\leq\; -\sqrt{2}\min_{j=1,\ldots,m}\{\lambda_{ij}\}V_i^{\frac{1}{2}}(\sigma_{ij}(t,\tilde{z}_{ij},x_{2i},\tilde{x}_j(t))), \quad \sigma_{ij}(t,\tilde{z}_{ij},x_{2i},\tilde{x}_j(t)) \in \mathbb{R}^m. \quad (12)$$

Thus, it follows from Theorem 4.1 in (Nersesov et al., 2009) that the siding surface $\mathscr{S}_i$ is finite-time stable. Furthermore, while on the sliding surface, the closed-loop dynamics for the ith agent are given by

$$\dot{\tilde{z}}_{ij}(t) \;=\; f_{1i}(t,\tilde{z}_{ij},x_{2i},\tilde{x}_j(t)) - \dot{\tilde{x}}_j(t), \quad \tilde{z}_i(0) = \tilde{z}_{i0}, \quad j \in \mathscr{O} \quad t \geq 0, \quad (13)$$

$$x_{2i}(t) \;=\; S_{1i}^{-1}(t,\tilde{z}_{ij})\left[S_{2i}(t,\tilde{z}_{ij})\dot{\tilde{x}}_j(t) - S_{3i}(t,\tilde{z}_{ij})\tilde{z}_{ij}(t) + \tilde{\sigma}_{ij}(t,\tilde{z}_{ij})\right], \quad (14)$$

and with the proper choice of the sliding surface structure (7), we can ensure that the reduced-order closed-loop dynamics (13) restricted to the surface exhibit stable limit cycles, thus guaranteeing obstacle avoidance.

The strategy for the obstacle avoidance along with the coordination control for the network of agents and the leader is described as follows. Consider the jth obstacle, where $j \in \mathscr{O}$. We define a prohibited region $\mathscr{P}_j \subset \mathbb{R}^{n-m}$ and a protected region $\mathscr{Q}_j \subset \mathscr{P}^{n-m}$ enclosing the ith obstacle, such that $\mathscr{P}_j \subset \mathscr{Q}_j$. The safe region of the jth obstacle is then defined as $\mathscr{R}_j \triangleq \mathbb{R}^{n-m} \setminus \mathscr{Q}_j$. We also define the jth periodic orbit as the boundary of the jth prohibited region, that is, $\Lambda_j \triangleq \partial\mathscr{P}_j$.

If the ith agent is in the protected region of the jth obstacle, that is, $\tilde{z}_{ij} \in \mathscr{Q}_j$, and if the direction of its velocity vector is towards $\mathscr{P}_j$, then the control strategy switches from the coordination control algorithm given in (Ghasemi and Nersesov, 2013) to the obstacle avoidance control algorithm given by (8). Therefore, the agent starts to act independently from the rest of the network and automatically all incoming connections from other agents are deactivated, that is in the connectivity graph G, all edges $(k,i) \in \mathscr{E}(G)$ for all $k \in \mathscr{V}(G)$ are disconnected. Next, for the resulting connectivity graph, we define a vertex set $\mathscr{V}_{\mathrm{L}} \subset \mathscr{V}(G)$ containing all agents for which there is at least one directed path from the leader and a vertex set $\mathscr{V}_i \subset \mathscr{V}(G)$ containing all agents for which there is no directed path from the leader. Note that $i \in \mathscr{V}_i$ and for all $u \in \mathscr{V}_{\mathrm{L}}$ and $v \in \mathscr{V}_i$, $(u,v) \notin \mathscr{E}(G)$. Next, we define an edge set $\mathscr{E}_{\mathrm{L}} \subset \mathscr{E}(G)$ containing all pairs $(u,v) \in \mathscr{E}(G)$, where $u,v \in \mathscr{V}_{\mathrm{L}}$. Respectively, we define an edge set $\mathscr{E}_i \subset \mathscr{E}(G)$ containing all pairs $(u,v) \in \mathscr{E}(G)$, where $u,v \in \mathscr{V}_i$. Thus, the resulting connectivity graph $\tilde{G}$ is partitioned to an up-stream sub-graph $\tilde{G}_{\mathrm{L}} \triangleq \{\mathscr{V}_{\mathrm{L}},\mathscr{E}_{\mathrm{L}}\}$ with the leader as its source and a down-stream sub-graph $\tilde{G}_i \triangleq \{\mathscr{V}_i,\mathscr{E}_i\}$ with the ith agent as its source (Figure 1).

For any of these sub-graphs, we identify the possible spanning trees $\tilde{G}_{\mathrm{L}}^*$ and $\tilde{G}_i^*$, respectively. Thus, the coordination control algorithm for $\tilde{G}_{\mathrm{L}}^*$, respectively $\tilde{G}_i^*$, ensure coordination among up-stream agents with respect to the leader, respectively among down-stream agents with respect to the ith agent. As soon as the obstacle is cleared, that is, the obstacle is not between the agent and its current desired position, then all the deactivated connections are restored and the control strategy switches back to the coordination control algorithm given in (Ghasemi and Nersesov, 2013) which ensures coordination among all agents with respect to the leader.

In case when the jth obstacle is an agent itself, then there is a possibility that the ith agent appears to be an obstacle for the jth agent too. Therefore, the down-stream subgraph $\tilde{G}_{ij}$ contains both the ith and the

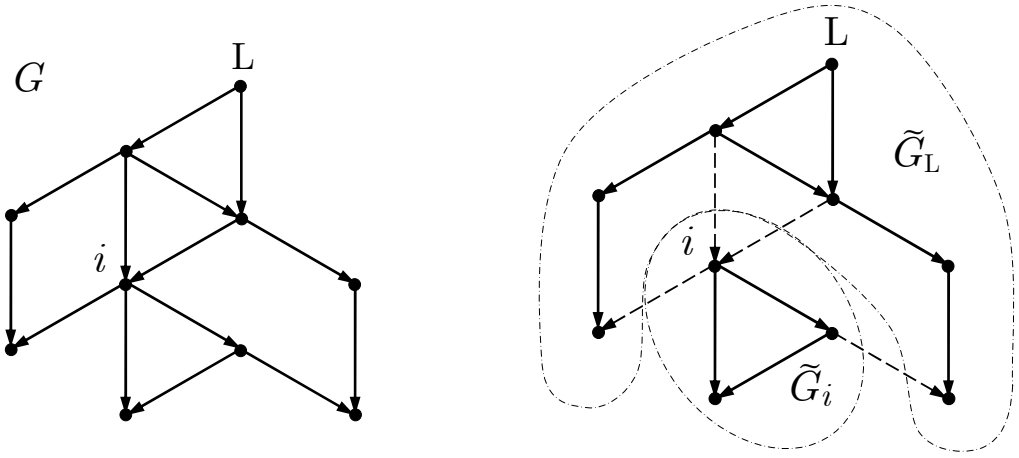

(a) Graph G (b) Sub-graphs $\tilde{G}_{\mathrm{L}}$ and $\tilde{G}_i$

Fig. 1. Information flow topology change due to obstacle avoidance.

jth agents as its sources. We might arbitrarily partition the subgraph $\tilde{G}_{ij}$ into $\tilde{G}_i$ and $\tilde{G}_j$ with the ith and the jth agents as their sources, respectively. Then, we can use the coordination control algorithm for any of the subgraphs, $\tilde{G}_{\mathrm{L}}$, $\tilde{G}_i$, and $\tilde{G}_j$ to avoid collisions.

As an example of the obstacle avoidance algorithm, consider the network of wheeled mobile robots with individual dynamics given in the previous section. We consider planar elliptical periodic orbits characterizing the prohibited boundaries for all obstacles in $\mathscr{O}$. We define the error states for the ith agent with respect to the jth obstacle as

$$\tilde{z}_{ij}(t) \triangleq [\tilde{z}_{xij}(t),\tilde{z}_{yij}(t),\tilde{z}_{\theta ij}(t)]^{\mathrm{T}} = [x_i(t)-\tilde{x}_j(t), y_i(t)-\tilde{y}_j(t), \theta_i(t)-\tilde{\theta}_j(t)]^{\mathrm{T}}, \quad j \in \mathscr{O}, \quad t \geq 0, \tag{15}$$

where $[\tilde{x}_j,\tilde{y}_j]^{\mathrm{T}}$ is the center position of the periodic orbit enclosing the jth obstacle, and $\tilde{\theta}_j \in \mathbb{R}$ is an arbitrary orientation assigned to the jth obstacle. Note that the definition of $\tilde{\theta}_j$ does not affect the behavior of the system on the periodic orbit and for the simplicity, we assume it is zero for all times. Accordingly, the error dynamics of the ith agent are given by

$$\dot{\tilde{z}}_{xij}(t) = v_{xi}(t)\cos\tilde{z}_{\theta ij}(t) - d\,\omega_i(t)\sin\tilde{z}_{\theta ij}(t) - \dot{\tilde{x}}_j(t), \quad \tilde{z}_{xij}(0) = \tilde{z}_{0xij}, \quad t \geq 0, \tag{16}$$

$$\dot{\tilde{z}}_{yij}(t) = v_{xi}(t)\sin\tilde{z}_{\theta ij}(t) + d\,\omega_i(t)\cos\tilde{z}_{\theta ij}(t) - \dot{\tilde{y}}_j(t), \quad \tilde{z}_{yij}(0) = \tilde{z}_{0yij}, \tag{17}$$

$$\dot{\tilde{z}}_{\theta ij}(t) = \omega_i(t), \quad \tilde{z}_{\theta ij}(0) = \tilde{z}_{0\theta ij}, \tag{18}$$

$$\dot{v}_{xi}(t) = \frac{m_i d}{\tilde{m}_i}\omega_i^2(t) + \frac{1}{\tilde{m}_i r_i}(\tau_{1i}(t)+\tau_{2i}(t)) + g_{1i}(t,\eta_{1i},\eta_{2i}), \quad v_{xi}(0) = v_{0xi}, \tag{19}$$

$$\dot{\omega}_i(t) = -\frac{m_i d}{\tilde{I}_i}\omega_i(t)v_{xi}(t) + \frac{a_i}{2\tilde{I}_i r_i}(\tau_{2i}(t)-\tau_{1i}(t)) + g_{2i}(t,\eta_{1i},\eta_{2i}), \quad \omega(0) = \omega_0, \tag{20}$$

Next, define functions $h_{ij} : \overline{\mathbb{R}}_+ \times \mathbb{R}^3 \to \mathbb{R}$ as

$$h_{ij}(t,\tilde{z}_{ij}) \triangleq \frac{1}{r_{1j}^2}(\cos\phi_j(t)\tilde{z}_{xij}(t) + \sin\phi_j(t)\tilde{z}_{yij}(t))^2 + \frac{1}{r_{2j}^2}(-\sin(t)\phi_j\tilde{z}_{xij}(t) + \cos\phi_j(t)\tilde{z}_{yij}(t))^2 - 1, \quad i = 1,\ldots,p, \quad j \in \mathscr{O}, \quad t \geq 0, \tag{21}$$

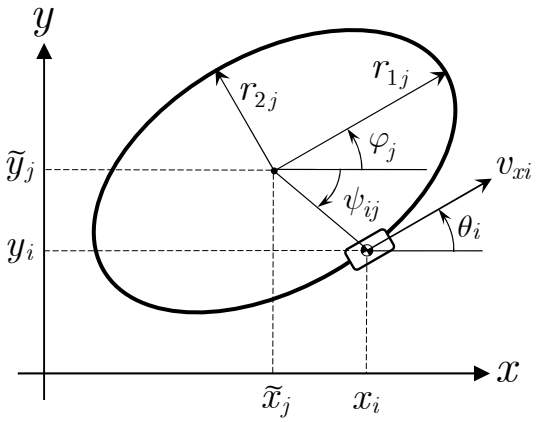

Fig. 2. An elliptical periodic orbit.

where $r_{1j}, r_{2j} \in \overline{\mathbb{R}}_+,\ j \in \mathscr{O}$ are the semi-major and the semi-minor axes of the elliptical periodic orbit enclosing the jth obstacle, respectively, and $\phi_j \in \mathbb{R},\ j \in \mathscr{O}$, is the orientation of the semi-major axis with respect to horizontal axis (Figure 2). Accordingly, we define the periodic orbit as the null space of $h_{ij}(\cdot,\cdot)$, that is,

$$\Lambda_{ij} \triangleq \{(t,\tilde{z}_{ij}) \in \overline{\mathbb{R}}_+ \times \mathbb{R}^3 : h_{ij}(t,\tilde{z}_{ij}) = 0\}. \tag{22}$$

Finally, the structure of the sliding surface (6) is chosen as follows, for $i = 1,\ldots,p$ and $j \in \mathscr{O}$,

$$S_{1ij}(t,\tilde{z}_{ij}) = \begin{bmatrix} \cos\tilde{z}_{\theta ij}(t) & -d\sin\tilde{z}_{\theta ij}(t) \\ \sin\tilde{z}_{\theta ij}(t) & d\cos\tilde{z}_{\theta ij}(t) \end{bmatrix}, \tag{23}$$

$$S_{2ij}(t,\tilde{z}_{ij}) = \begin{bmatrix} 1 & 0 & 0 \\ 0 & 1 & 0 \end{bmatrix}, \tag{24}$$

$$\tilde{\sigma}_{ij}(t,\tilde{z}_{ij}) = -H_{ij}(t,\tilde{z}_{ij}) + \tilde{C}_{ij}(t)\tilde{z}_{ij}(t)h_{ij}(t,\tilde{z}_{ij}), \tag{25}$$

where

$$H_{ij}(t,\tilde{z}_{ij}) \triangleq \begin{bmatrix} -\tilde{z}_{yij}\dot{\phi}_j(t) + \frac{\dot{\psi}_{ij}(t)}{r_{1j}r_{2j}}(\tilde{h}_{1j}(t)\tilde{z}_{xij} - \tilde{h}_{2j}(t)\tilde{z}_{yij}) \\ \tilde{z}_{xij}\dot{\phi}_j(t) + \frac{\dot{\psi}_{ij}(t)}{r_{1j}r_{2j}}(\tilde{h}_{3j}(t)\tilde{z}_{xij} - \tilde{h}_{1j}(t)\tilde{z}_{yij}) \end{bmatrix}, \tag{26}$$

$$\tilde{h}_{1j}(t) \triangleq (r_{1j}^2 - r_{2j}^2)\sin\phi_j(t)\cos\phi_j(t), \tag{27}$$

$$\tilde{h}_{2j}(t) \triangleq r_{1j}^2\cos^2\phi_j(t) + r_{2j}^2\sin^2\phi_j(t), \tag{28}$$

$$\tilde{h}_{3j}(t) \triangleq r_{1j}^2\sin^2\phi_j(t) + r_{2j}^2\cos^2\phi_j(t), \tag{29}$$

$\psi_{ij}(\cdot) \in \mathbb{R}_+$ is a monotonically increasing positive function of time which describes the rotation of the agent around the periodic orbit, and

$$\tilde{C}_{ij}(t) \triangleq \begin{bmatrix} \tilde{c}_{1ij}(t) & 0 & 0 \\ 0 & \tilde{c}_{2ij}(t) & 0 \end{bmatrix}, \tag{30}$$

with $\tilde{c}_{1ij}(\cdot),\ \tilde{c}_{2ij}(\cdot) \in \mathbb{R}_+$ are monotonically increasing positive functions of time which define the convergence rate toward the periodic orbit. Note that ψ_{ij}, $\tilde{c}_{1ij}$ and $\tilde{c}_{2ij}$ are in fact some bounded time-varying gains allowing a smooth transition to the periodic orbit (Soltan et al., 2011).

Fig. 3. Experimental differential drive wheeled mobile robots.

Thus, the sliding mode controller (8) guarantees finite time convergence to the sliding surface; while, on the sliding surface, the reduced-order dynamics exhibit a stable limit cycle (Soltan et al., 2011) which ensures obstacle avoidance.

4. Experimental Validation

We validate the above results using two experimental wheeled mobile robots shown in Figure 3. The robot wheels are driven by two DC motors which are controlled by a Pandaboard single-board computer running a Linux® operating system and an Arduino™ microcontroller board. The control program is built in The MathWorks™ Simulink® environment. Through the Simulink® Real-Time Workshop®, the program is compiled and built as a real-time executable for the Pandaboard target (Fabian and Clayton, 2012). The communication between the PC and the Pandaboard is done via wireless connection. We use a black and white 640×480-resolution COHU-2672 camera equipped with a Data Transitions DT3120 frame grabber to capture overhead image frames in order to identify robot positions that will be used in our feedback measurements. The camera is installed 2.86 m above the floor. To ensure that there is no delay throughout the experiment, the frames rate is set at 2fps. Since the captured image is distorted, a calibration process is used to allow the true real-world position of every point in the image to be calculated.

We consider the coordination problem in which the first robot is leading the formation while communicating its state information with the second robot. The objective is to keep robots in parallel formation with respect to the y axis. The leader agent is set to move along a sinusoidal path with a constant velocity according to $y_{\mathrm{L}}(t) = 0.2\sin(\pi x_{\mathrm{L}}(t))$, $(\dot{x}_{\mathrm{L}}^2(t) + \dot{y}_{\mathrm{L}}^2(t))^{\frac{1}{2}} = 0.05$ m/sec, $t \geq 0$. Two stationary obstacles are placed on the way of the robots with their center positions located at $[1, -0.2]^{\mathrm{T}}$ and $[1.5, 1.2]^{\mathrm{T}}$ and their orientations being $2\pi/3$ and $\pi/3$, respectively. Figure 4 (a) shows the position phase portrait with the robots orientations and Figure 4 (b) shows the time history of the control torques acting on both wheels of each robot with τ_{1i} and τ_{2i} being the control torques acting on the left and the right wheels of the ith robot, respectively.

5. Conclusion

In this paper, we extended the cooperative control technique for multiagent systems developed in (Ghasemi and Nersesov, 2013) by incorporating it with the obstacle/collision avoidance algorithm. Obstacle avoidance is achieved by surrounding the stationary as well as moving obstacles by elliptical or other convex shapes that serve as stable periodic solutions to planar systems of ordinary differential equations and using

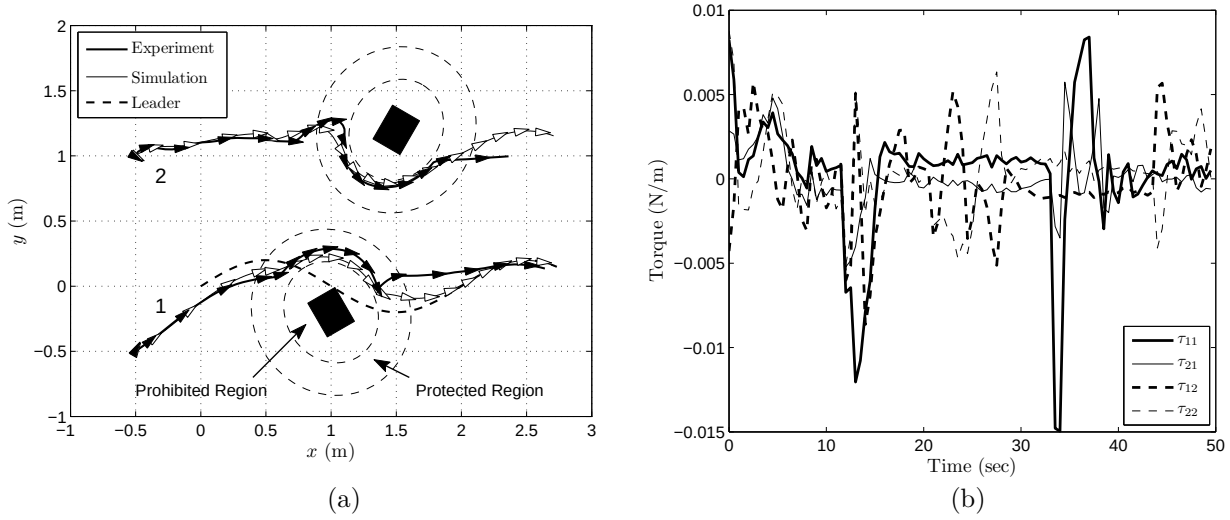

Fig. 4. (a) Position phase portrait with orientation of the robots, (b) Control torques versus time.

transient trajectories of those systems to navigate the agents around the obstacles. Experimental validation demonstrated the efficacy of our theoretical approach.

References

Bullo, F., Cortéz, J., and Martinéz, S. (2009). *Distributed Control of Robotic Networks*. Princeton University Press, Princeton, NJ.

Fabian, J. and Clayton, G. (October 2012). One-point visual odometry using a RGB-depth camera pair. In *Proc. ASME Dyn. Sys. Contr. Conf.*, pages DSCC2012–MOVIC2012–8700, Fort Lauderdale, FL.

Ghasemi, M. and Nersesov, S. (October 2013). Sliding mode coordination control design for multiagent systems. In *Proc. ASME Dyn. Sys. Contr. Conf.*, pages DSCC2013–3902, Palo Alto, CA.

Nersesov, S. G., Nataraj, C., and Avis, J. M. (2009). Design of finite-time stabilizing controllers for nonlinear dynamical systems. *Int. J. Robust and Nonlinear Control*, 19:900–918.

Porfiri, M., Robertson, D., and Stilwell, D. (2007). Tracking and formation control of multiple autonomous agents: a two-level consensus approach. *Automatica*, 43(8):1318–1328.

Ren, W. and Beard, R. W. (2008). *Distributed Consensus in Multi-Vehicle Cooperative Control*. Springer-Verlag, London, UK.

Soltan, R. A., Ashrafiuon, H., and Muske, K. R. (2011). ODE based obstacle avoidance and trajectory planning for unmanned surface vessels. *Robotica*, 29(5):691–703.

Utkin, V. I. (1977). Variable structure systems with sliding modes. *IEEE Trans. Auto. Contrl.*, 22:212–222.